EMERGENCE OF A TWISTED MAGNETIC FLUX BUNDLE AS A SOURCE OF STRONG FLARE ACTIVITY

TAKAKO T. ISHII[1,2] , HIROKI KUROKAWA[1] AND
TSUTOMU T. TAKEUCHI[2,3]

[1] Kwasan and Hida Observatories, Kyoto University, Yamashina-ku, Kyoto 607, JAPAN

[2] Department of Astronomy, Kyoto University, Sakyo-ku, Kyoto 606-01, JAPAN

[3] Research Fellow of the Japan Society for the Promotion of Science

E-mail: ishii@kusastro.kyoto-u.ac.jp

ABSTRACT

Sunspot proper motions and flares of a super active region NOAA 5395, which was the biggest and the most flare-active region in the 22nd sunspot cycle, were analyzed in details. We measured sunspot proper motions by using the $H\alpha - 5.0$ Å images obtained with the 60-cm Domeless Solar Telescope (DST) at Hida Observatory, Kyoto University and found some peculiar vortex-like motions of small satellite spots successively emerged from the leading edge of this sunspot group. To explain these motions of small sunspots, we proposed a schematic model of the successive emergence of twisted and winding magnetic flux loops coiling around a trunk of magnetic flux tube. The location of the strongest flare activity was found to coincide with very the site of the vortex-like motions of sunspots. We conclude that the flare-productive magnetic shear is produced by the emergence of the twisted magnetic flux bundle. Magnetic energy is stored in the twisted flux bundle which is originally formed in the convection zone and released as flares in the course of the emergence of the twisted flux bundle above the photosphere.

Subject headings: Sun : activity — Sun : flares — Sun : sunspots

1. INTRODUCTION

Characteristics of flare-productive sunspot groups have been studied by many authors (Zirin & Tanaka 1973; Hagyard et al. 1984; Kurokawa 1987; Zirin & Liggett 1987; Tanaka 1991; and Kurokawa 1991, 1996). In these studies, the authors pointed out that sheared configuration of magnetic field and δ-type configuration of sunspot group are essential characteristics for strong flare activities.

From statistical studies, however, Shi & Wang (1994) found that 23 % of δ-type sunspot groups produced X-class flares, and Chen et al. (1994) found that even strong magnetic shear of more than 80-degree shear angle is not a sufficient condition to produce flares.

On the other hand, Tanaka (1991) suggested that an emergence of a twisted magnetic flux rope produces strong flares. Kurokawa (1987, 1991, 1996) also concluded that strong flare activities occur whenever a magnetic shear is rapidly developed by a successive emergence of twisted magnetic loops. Zirin & Liggett (1987) showed that big flares occurred in δ-groups which emerged as continents.

These studies suggest that flare-productivity of a sunspot group depends on formation process of the δ-type configuration or the magnetic shear. This processes can be examined by measuring of sunspot proper motions.

A large active region observed in March 1989 (NOAA 5395) was a highly flare-productive sunspot group with δ-type configuration. The region produced about two hundred flares including ten X-class flares. All X-class flares were observed in three particular regions. Wang et al. (1991) studied this region using Magnetograms, Dopplergrams and monochromatic images mainly obtained at Big Bear Solar Observatory (BBSO) and Zhang (1995) also studied using Magnetograms obtained at Huairou Solar Observing Station (HSO).

We measured proper motions of sunspots in NOAA 5395 by using Hα images obtained with the 60-cm Domeless Solar Telescope (DST) at Hida Observatory, Kyoto University in order to study the formation process of δ-type configuration and magnetic shear in the region. In this study we demonstrate that twisted magnetic flux tubes successively emerged at the preceding edge of the great sunspot group and that they played an essential role in the production of strong flare activities of NOAA 5395.

We describe the procedure of data analysis in Sec. 2 and show the obtained results of sunspot proper motions in Sec. 3. In Sec. 4 we discuss the cause of peculiar sunspot motions found at the leading edge of the active region and propose a morphological model of an emerging twisted magnetic flux bundle which is essential to the strong flare activity. Section 5 is devoted for our conclusion.

2. DATA ANALYSIS

2.1. Observational Data

The active region NOAA 5395 turned into the visible hemisphere on March 6 and turned off behind the western limb on March 19. During this period, except on March 7, 13 and 17, we continuously observed the evolution of the region with DST. Many Hα monochromatic images were sequentially obtained with the Zeiss Lyot filter of 0.25 Å passband and a Nikon motor-drive film camera of DST in 10 wavelength (*i.e.* Hα ± 0.0 Å, ±0.3 Å, ±0.5 Å, ±0.8 Å, ±1.2 Å and −5.0 Å). In this study we mainly used Hα − 5.0 Å images to measure sunspot proper motions.

We digitized the film densities of the Hα − 5.0 Å images by a film scanner and analyzed them by using IDL (Interactive Data Language) software on a personal computer and UNIX. Times and numbers of measured images are listed in Table 1. One example of

the Hα − 5.0 Å images is shown in Fig. 1.

We carefully identified individual sunspot umbrae of the group in successive images and gave numbers to them as shown in Fig. 1b, where the signs F and f stand for the *following* magnetic polarity, P and p, the *preceding* polarity and the sign " : " means uncertainness. We used the magnetograph data supplied by Okayama Astrophysical Observatory (OAO), BBSO and HSO for the determination of magnetic polarities of the sunspots.

2.2.   Calculation of Latitude and Carrington Longitude of Sunspot Umbrae

The field of view of the Hα filtergraph of DST is a circle of about 390 ″ diameter. The heliocentric coordinate of the center of the circle is recorded for each observation.

Referring to the center of the circle, we determined the heliocentric coordinate of individual sunspot umbra in IDL pictures. The umbra position was defined as the center of gravity position of the umbra, which is determined by drawing the density contour of each umbra in an IDL picture. By means of coordinate transformation we finally obtained heliographic latitude and Carrington longitude of each umbra.

During this observation the pointing accuracy of DST was about 10 ″, and this limits the accuracy of absolute positions of umbrae. Then we defined the center of gravity of a triangle made by three umbrae F1, F3 and P1 as a reference point and determined the relative positions of all sunspot umbrae referred to this point. The mean heliographic latitude of the reference point averaged over all measured images is 33.°6 N and its standard deviation is 1.0 degree. By excluding the images whose deviation exceeds 1σ, we get 33.°5 N as the average latitude of the reference point.

The longitudinal positions are significantly influenced by the differential rotation.

Tang(1981) gave the differential rotation rate for the sunspot groups at high ($28° \sim 40°$) latitude by the formula

$$\Omega = 14.37 - 2.60 \sin^2 \theta \quad \text{deg/day}, \tag{1}$$

where Ω is the sidereal rotation rate. We would like to know the synodic rotation rate. According to Zirin (1989), the synodic rotation rate (ω) and the sidereal rate (Ω) differ by the Earth's orbital velocity of 0.9865 deg/day;

$$\omega = \Omega - 0.9865 \quad \text{deg/day}. \tag{2}$$

And we find that the synodic rotation rate at the latitude of 33.°5 N is 12.59 deg/day.

On the other hand, the heliographic longitude of the disk center (L_0) decreased by the rate of 13.18 deg/day. Considering the difference of above two values (i.e. 12.59 deg/day and 13.18 deg/day), the Carrington longitude of the reference point should change by the rate of 0.59 deg/day due to the differential rotation.

We first determined the heliographic latitude and Carrington longitude of the reference point for the image of 00:00 UT of Mrach 11, which are 33.°5 N (latitude) and 254.°5 L (longitude) respectively. Then for all other images we calculated the Carrington longitude of the reference point by correcting the value of 0.59 deg/day. For each sunspot umbra, we adapted a different correction rate for the differential rotation corresponding to its latitude. After these corrections for the differential rotation, we calculated velocities of proper motions of sunspot umbrae. The term of umbra velocity used hereafter in this paper means a velocity of proper motion.

3. RESULTS

We noticed that the motion of F1 is quite different from those of other big umbrae (F3, F4 and P1); the umbra F1 moved southward or southwestward, while the others moved

eastward or northwestward. The umbrae F3, F4 and P1 moved toward east at velocities of 0.03 ∼ 0.08 km/s. The umbra F1 moved southwestward at a velocity of about 0.05 km/s and it suddenly accelerated after 12 March. The velocity of F1 reached at 0.11 km/s on March 14. The other three big umbrae moved eastward at velocities of 0.03 ∼ 0.08 km/s. These velocities are approximately the same as those of previous works, in which sunspot proper motions were measured in various active regions (van Driel-Gesztelyi & Petrovay 1990, van Driel-Gesztelyi et al. 1993, van Driel-Gesztelyi et al. 1994, Schmieder et al. 1994, and Herdiwijaya, Makita, & Anwar 1997).

According to Herdiwijaya et al. (1997), the longitudinal velocities of sunspots varies with their Zürich classes; the average velocity of GHJ classes (i.e. decaying phase) is smaller than that of AB classes (i.e. emerging phase). The following polarity sunspots of Zürich AB classes show the average longitudinal velocity of 88 m/s. On the other hand, the average longitudinal velocities of EF classes (i.e. well-developed phase) and GHJ classes are 18 m/s and 21 m/s respectively. The average longitudinal velocity of following polarity spot F1 is 57 m/s for the period from 9 to 15 March. This means that the magnetic flux tube forming sunspot F1 is still emerging from the subphotospheric layer in our observation period.

We also noticed conspicuous motions of small sunspot umbrae around the leading sunspot F1. They successively appeared at the south and southeast edge of F1 and moved eastward. We examined their motions in details. By calculating the displacements of these small umbrae between successive frames of images in each day, we determined their velocities of proper motions. We also calculated their velocities relative to F1 (relative velocities, hereafter). The results obtained only for images of good seeing are presented in Fig. 2, where arrows indicate the relative velocities of the small umbrae.

On March 9 (Fig. 2a), small umbrae near F1 (p1 and p2) moved southward and others (p3, p4 and p5) moved eastward. The relative velocities of these umbrae were all

0.15 km/s. On March 10 (Fig. 2b), small umbrae (p:6, f:1) near F1 moved southward at relative velocities of 0.15 and 0.30 km/s, respectively. A p-polarity umbra (p7) moved southeastward at a relative velocity of 0.10 km/s. A p-polarity umbra (p9), which moved toward P1, had a relative velocity of 0.20 km/s. A p-polarity umbra (p8) moved eastward at a relative velocity of 0.10 km/s. Small umbrae at the north side of F1 moved eastward along the channel between F1 and F2. On March 11 (Fig. 2c), small umbrae at the east and the southeast sides of F1 moved eastward or northeastward at relative velocities of 0.30 ∼ 0.40 km/s. Small umbrae at the north side and at the west side of F1 (f-polarities) also moved eastward or northeastward. On March 12 (Fig. 2d), small umbrae at the east and southeast side of F1 also moved eastward at much higher relative velocities of 0.30 ∼ 0.60 km/s. Small umbrae (f-polarities) at the north side and at the northwest side of F1 also moved east or northeast along the north edge of F1.

We also calculated the relative velocities of proper motions of the small umbrae by using all available images for each day. The average velocities obtained in each day are given in Fig. 3. It is found that the two results of Fig. 2 and Fig. 3 agree with each other. From these results we summarize main characteristics of proper motions of small umbrae as follows.

At the south and southeast edges of F1, small umbrae successively emerged and moved toward P1 through the east side of F1. Appearing near F1, they first moved southward, turned to the east and finally moved northeastward to approach P1. It means they moved along curved trajectory like an outflowing vortex. Such emergences and motions of small sunspots continued with their speed accelerated from 9 through 12 of March. Spot P1 became bigger in its umbra area from 10 through 12, March. Wang et al. (1991) also found that p-polarity umbrae at the east side of F1 merged into P1. We found that spot P2 newly formed on 14 Mar at the region where small emerging sunspots or emerging magnetic flux

successively converged from 12 through 14 March (see Fig. 1b).

Some small umbrae emerging at the south west edge of F1 (i.e. f6, f10, f11, f13, f14, and f15) first moved northward at the west side of F1 and moved eastward or northeastward along the north edge of F1 from Mar 10 through 12. They converged into a few larger umbrae at the northeast side of F1 on March 12. By March 14 the northeast part of F1 has been separated from its leading part and moved northeastward to form F5 umbra.

4. DISCUSSIONS

4.1. A Schematic Model of Emerging Twisted Flux Tubes

The most remarkable result found in the previous section is the vortex-like motions of small sunspot umbrae around the leading sunspot F1. Pairs of small umbrae of different magnetic polarities successively emerged at the leading edge of F1 (i.e. at the south or southwest edges of F1) from 9 through 12, March. These umbrae moved clockwise toward the southwest of P1, where growth of P1 was observed from 10 through 12, March and P2 was formed on March 14. At the west and north sides of F1, small umbrae moved anticlockwise and formed F5 by merging with some parts of decaying F1. These motions are schematically summarized in Fig. 4a. At the east side of F1, small umbrae, most of which are p-polarities, moved clockwise and formed P2. At the west and north sides of F1, small umbrae, all f-polarities, moved anticlockwise and formed F5 by merging with some parts of decaying F1. Notice vortex-like lines and structures of small sunspot umbrae and penumbrae surrounding F1 spot in Fig. 1a. Wang et al. (1991) also found the same vortex-like motions of magnetic features in this region using Magnetograph data.

For the explanation of these peculiar vortex-like motions, we propose a schematic model of emerging twisted flux tubes given in Fig. 4b. The model is characterized by the

successive emergence of twisted flux tubes coiling around the main trunk of flux tube F1. The bundle of flux tubes is twisted and each flux tube is also twisted. As Parker (1955) pointed out, the magnetic buoyancy raises up the system of twisted magnetic-flux bundle.

The successive emergence of the inclined and twisted flux bundle can explain the vortex-like motions of small sunspots both at the southeast and the northwest sides of F1 as shown in Fig. 4a. In Fig. 4b planes P_{t_1} and P_{t_2} show the positions of the photosphere relative to the emerging flux tubes for the different days. The cross sections of flux tubes on each photospheric plane correspond to sunspots. As the coiling loops successively emerge, the small p-polarity and f-polarity sunspots can be seen to move clockwise and anticlockwise, at the southeast side and at the northwest side of F1 respectively. Notice that small p-polarity sunspots seen on the planes P_{t_1} are all converged into the sunspots P2 on P_{t_2} and that f-polarity ones are converged into the sunspot F5. These are very consistent with the observations summarized at the beginning of this section.

In addition, it is interesting to notice another evolutional feature of F1. As studied in section 3, the southwestward motion of the umbra F1 suddenly accelerated after 12 March. We observed the drastic change of the shape of F1 at the same time (see Fig 1b); F1 suddenly elongated and started to decay after 12 March. We also observed the rapid growth of P2 and F5 umbrae between 12 and 14 March. This time coincidence between the decay of F1 and the growth of P2 and F5 strongly suggests a close causal relation between them : The umbrae F1 was stable until 12 March because it was bound by the coiling flux tubes. When the coiling flux tubes already emerged above the photosphere after 12 March, however, the trunk of flux tube F1 suddenly expanded, or elongated and started to decay.

Furthermore, it must be worthwhile here to mention about a differential emergence of magnetic loops. Suppose the gas pressure and magnetic field strength in the tube are p_i and B_i and the surrounding external pressure at the same height is p_e. Then the lateral

total pressure balance implies

$$p_{\rm e} = p_{\rm i} + \frac{B_{\rm i}^2}{8\pi}. \tag{3}$$

If the temperature (T) is uniform and the corresponding densities are $\rho_{\rm i}, \rho_{\rm e}$, Equation (3) becomes

$$\frac{k_{\rm B}T\rho_{\rm e}}{m} = \frac{k_{\rm B}T\rho_{\rm i}}{m} + \frac{B_{\rm i}^2}{8\pi}, \tag{4}$$

where we take the perfect gas law ; $p = k_{\rm B}\rho T/m$ ($k_{\rm B}$ is the Boltzmann constant and m is the mean particle mass). The plasma in the tube feels a resultant buoyancy force of $(\rho_{\rm e} - \rho_{\rm i})g$ per unit volume, which tends to make the tube rise.

The trunk and coiling loops in Fig 4b are considered to have different magnetic pressures ($B_{\rm i}$) and different densities ($\rho_{\rm i}$). Different densities give different buoyancy force, so the system rises differentially. Difference of the shapes of flux tubes (i.e. different curvatures of flux tubes) may also make the system rise differentially.

In spite of this consideration, the schematic drawing like Fig. 4b may give the impression that the whole system emerges at the same speed, because we do not draw how differentially the loops rise. We need more observational data of better temporal- and spatial- resolutions before we can discuss more realistic structures of successively emerging flux loops. And this is an important subject to be attacked in future works. Figure 4b, however, well shows the essential characteristics of our model, i.e. an emergence of a twisted magnetic flux bundle. It does not influence our conclusion how differentially the flux loops rise.

4.2. Flare Activity in NOAA 5395

According to Solar Geophysical Data (SGD), about two hundred flares occurred in this active region. Some example of flares observed with DST at Hida Observatory are shown in

Fig. 5. The positions of the flares given in SGD were transformed to our coordinate system (heliographic latitudes and Carrington longitude) and these of the flares stronger than C-class in soft X-ray importance were plotted in Fig. 6, where the positions of the flares are given for each day (from 15:00 UT of the previous day to 15:00 UT of the day). The relative velocities of the small sunspot umbra around F1 are also shown in Fig. 6. Notice that almost all flares occurred around F1 from 9 through 12 March. On 15 March, before which the twisted flux bundle has already emerged out, however, no strong flare occurred around F1 (Fig. 6). On the contrary, some strong flares occurred along the sheared neutral line formed between P2 and F5 on 14 and 15 March.

Especially noticeable in these two figures (Fig. 5 and 6) is that from 9 through 12, March, many M-class and C-class flares occurred at the leading edge and at the east of F1 where the vortex-like motions of the small umbrae were found. The north side of F1 is also flare-productive especially on 12 March. These results strongly suggest that the vortex motions of small spots around F1 or the successive emergence of twisted magnetic flux tubes should be sources of the strong flare activities in this region.

4.3. Flare Energy Build-up Process

The vortex-like motions of small satellite spots around F1 were explained with emergences of the twisted magnetic flux bundle(Sec. 4.1), and strong flare activities preferentially occurred around this emerging flux region (Sec. 4.2). These evidence strongly suggest the existence of causal relations between the emergences of twisted magnetic flux tubes and the strong flare activities. With successive emergence of twisted flux tubes, very complex magnetic field structures, which consist of many current loops, were formed around F1 and at the south of P1. Notice the twisted dark loops at the east side of F1 in the Hα images of Fig. 7. They have different orientations with each other, and they are considered

to reconnect with each other and sometimes to produce flares as shown in Fig. 5.

In the convection zone, magnetic flux tubes are intensified by a dynamo action and twisted by convection in a rotating fluid. When the twisted flux tubes emerge to the photosphere, the twists should get loose as shown in Fig. 4 with decrement of the gas pressure. Since the twisted magnetic tubes store much energy, the energy could be released in the violent flare activities in the F1 region of NOAA 5395.

The idea that twisted magnetic flux tubes store the energy for flares is first proposed by Piddington (1974), and several observational studies developing this idea have been published by Tanaka (1991), Kurokawa (1987, 1991, 1996), Wang (1994) and Wang et al. (1996). Our study presents another clear evidence of the emergence of a strongly twisted and flare-productive magnetic flux bundle. Especially important findings in this study are the outflowing vortex-like motions of small sunspots and extremely hot flare activity around the leading sunspot F1. Such conspicuous motions of sunspots and associated hot flare activities have been hardly reported before, though Kurokawa et al. (1987) noticed a conspicuous growth of the leading part of δ-type sunspot just before a great flare of April 25, 1984 in NOAA 4474. Leka et al. (1994, 1996) also reported some vortex-like motions of small sunspots in an emerging flux region, but the region is not so active in flare production. More examinations of the relation between the vortex motions of sunspot structures and flare activity are necessary in future observations and measurements of existing data.

5.   CONCLUSION

Sunspot proper motions and flares of a super active region NOAA 5395, which is one of the biggest and the most flare-active regions in the 22nd sunspot cycle, were analyzed in details. We measured the sunspot proper motions by using the Hα images obtained

with DST and found some peculiar vortex-like motions of small satellite spots successively emerging from the leading sunspot F1. For the explanation of these motions of small sunspots, we proposed a schematic model of the successive emergence of twisted and winding magnetic flux loops coiling around a trunk of magnetic flux tube (Fig 4).

We also found most of flares preferentially occurred in this emerging region around F1. These results are consistent with our previous conclusion that the flare productive magnetic shear is produced by the emergence of twisted magnetic flux tubes (Kurokawa 1987, 1991, 1996). This study strongly suggests that the magnetic energy of a flare-productive sunspot group is stored in a twisted flux bundle which is originally formed in the convection zone. The energy is released as flares in the course of the emergence of the twisted flux bundle above the photosphere.

Studies of the typical flux tube geometry which has enough energy for big flares should be useful for forecasting flare occurrence. It is still unclear, however, which type of emergence of twisted flux tube always produces strong flare activity. We need more observational studies of the process of magnetic shear developments in more active regions by using proper motions of sunspots and evolutional changes of Hα fine structures and photospheric vector magnetic field.

REFERENCES

Chen, J., Wang, H., Zirin, H., & Ai, G. 1994, Sol. Phys., 154, 261

Hagyard, M. J., Smith, Jr. J. B., Teuber, D. & West, E. A., 1984, Sol. Phys., 91, 115

Herdiwijaya, D., Makita, M., & Anwar, B. 1997, PASJ, 49, 235

Kurokawa, H. 1987, Sol. Phys., 113, 259

Kurokawa, H. 1991, Lecture Notes in Physics, 387, 39

Kurokawa, H. 1996, in Magnetodynamic Phenomena in the Solar Atmosphere
— Prototypes of Stellar Magnetic Activity , ed. Y. Uchida et al. pp.185 - 194.

Kurokawa, H., Hanaoka, Y., Shibata, K., & Uchida, Y. 1987, Sol. Phys., 108, 251

Leka, K. D., van Driel-Gesztelyi, L., Nitta, N., Canfield, R. C., Mickey, D. L., Sakurai, T.,
& Ichimoto, K. 1994, Sol. Phys., 155, 301

Leka, K. D., Canfiield, R. C., McClymont, A. N., & van Driel-Gesztelyi, L., 1996, ApJ, 463,
547

Parker, E. N. 1955, ApJ, 121, 491

Piddington, J. H. 1974, Sol. Phys., 38, 465

Schmieder B., Hagyard, M. J., Ai, G., Zhang, H., Györi, B. K. L., Rompolt, B., Démoulin,
P., & Machado, M. E. 1994, Sol. Phys., 150, 199

Shi, Z. & Wang, J. 1994, Sol. Phys., 149, 105

Solar Geophysical Data 1989, Nos. 537(I), 541(II)

Tanaka, K. 1991, Sol. Phys., 136, 133

Tang, F. 1981, Sol. Phys., 69, 399

van Driel-Gesztelyi, L. & Petrovay, K. 1990, Sol. Phys., 126, 285

van Driel-Gesztelyi, L., Csepura, G., Nagy, I., Gerlei, O., Schmieder, B., Rayrole, J., & Demoulin, P. 1993, Sol. Phys., 145, 77

van Driel-Gesztelyi, L., Hofmann, A., Demoulin, P., Schmieder, B., & Csepura, G. 1994, Sol. Phys., 149, 309

Wang, H., Tang, F., Zirin, H., & Ai, G. 1991, ApJ, 380, 282

Wang, J. 1994, Sol. Phys., 155, 285

Wang, J., Shi, J., Wang, H., & Lü, Y. 1996, ApJ, 456, 861

Zhang, H. 1995, A&AS, 111, 27

Zirin, H. & Liggett, M. 1987, Sol. Phys., 113, 267

Zirin, H. & Tanaka, K. 1973, Sol. Phys., 32, 173

Zirin, H. 1989, Astrophysics of the Sun, (Cambridge: Cambridge Univ. Press)

Fig. 1.— The Hα − 5.0 Å image obtained with DST at 23:19 on March 11. Notice the vortex-like lines of small umbrae and penumbra structures surrounding a large sunspot umbra F1. (b) Daily evolutional changes of NOAA 5395. North is up, west is to right. An interval of two hair lines corresponds to 100 ″. Sunspots measured their proper motions are given numbers. the signs F and f stand for the *following* polarity and the P and p, the *preceding* polarity. the sign " : " means uncertainness. This region was elongated toward southwest and northeast.

Fig. 2.— Velocities of small umbrae relative to F1 measured for two images of good seeing. An arrow in the upper right corner of each panel indicates the velocity scale of 100 m/s. Vortex-like motions of small satellite spots are found. (a) From 23:31 UT on March 8 to 05:10 UT on March 9. (b) From 00:37 UT to 05:46 UT on March 10. (c) From 23:24 UT on March 10 to 01:28 UT on March 11. (d) From 23:18 UT on March 11 to 02:48 UT on March 12.

Fig. 3.— The same as Fig. 2 but for all images on a day.

Fig. 4.— (a) Schematic summary of observed vortex-like motions of small umbrae surrounding F1. Pairs of small umbrae successively emerged at the leading edge of F1. At the east side of F1, small umbrae, mainly p-polarities, moved clockwise and formed P2. At the west and north sides of F1, small umbrae, all f-polarities, moved anticlockwise and formed F5 by merging with some parts of decaying F1. (b) A schematic model of emerging flux tubes. The bundle of flux tubes is twisted and each flux tube is also twisted. Planes P_{t_1} and P_{t_2} show the positions of the photosphere relative to the emerging flux tubes for the different days. The cross section of flux tubes on each photospheric plane correspond to sunspots.

Fig. 5.— Examples of Hα flares observed with DST at Hida Observatory. Most of flares during 9 – 12 March occurred at the east side and leading edge of F1.

Fig. 6.— Flare positions and relative velocities of small umbrae to F1. Almost all flares occurred around F1 from 9 through 12 March. On March 9 and 11, many M-class and C-class flares occurred at the east side of F1. On 15 March, before which the twisted magnetic flux bundle has already emerged out, no strong flare occurred around F1.

Fig. 7.— H$\alpha \pm 0.0$ Å images obtained at (a) 02:31 UT 11 March (b) 00:14 UT 12 March. Notice the twisted dark loops at the east side of F1. They have different orientations with each other, and they sometimes reconnect with each other to produce flares as shown in Fig. 5.

Table 1: Observational log

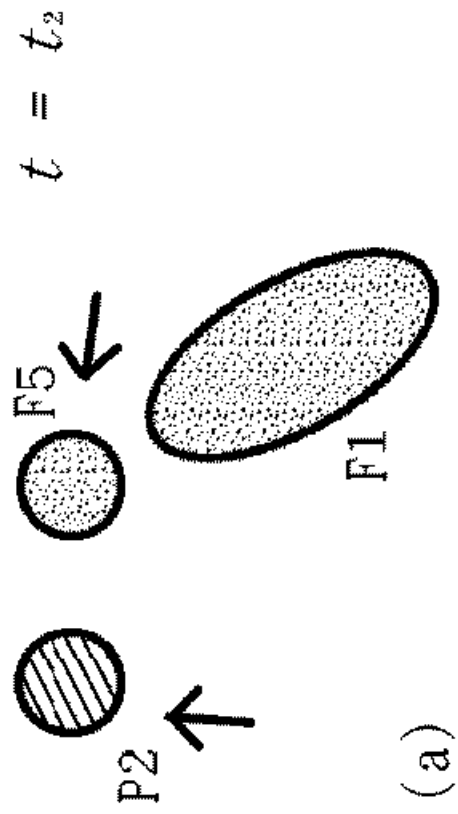| date	observation time (UT)	number of images
March 9	22:54 $\sim$ 07:29	11
10	22:36 $\sim$ 06:58	5
11	22:30 $\sim$ 02:01	7
12	22:18 $\sim$ 04:39	6
14	03:32 $\sim$ 06:33	2
15	22:21 $\sim$ 05:57	7

This figure "fig1a.gif" is available in "gif" format from:

http://arXiv.org/ps/astro-ph/9708208v2

This figure "fig1b.gif" is available in "gif" format from:

http://arXiv.org/ps/astro-ph/9708208v2

$t = t_1$

f

f

f

p

p

p

F1

× Leading edge

$t = t_2$

F5

F1

P2

(a)

P_{t_i} : photosphere at $t = t_i$

P_{t_1}

P_{t_2}

f f

f

F1

p

p

F5

F1

P2
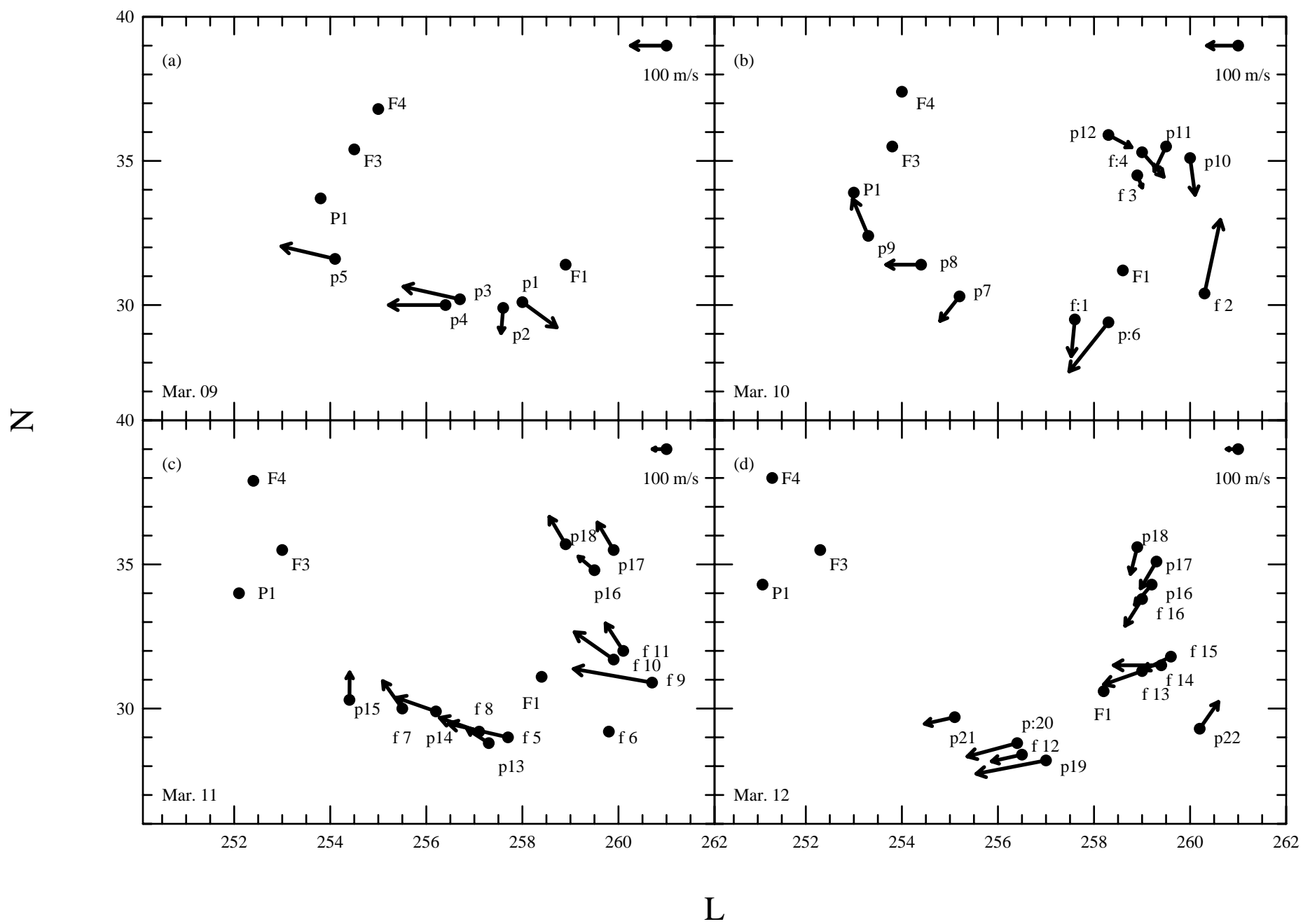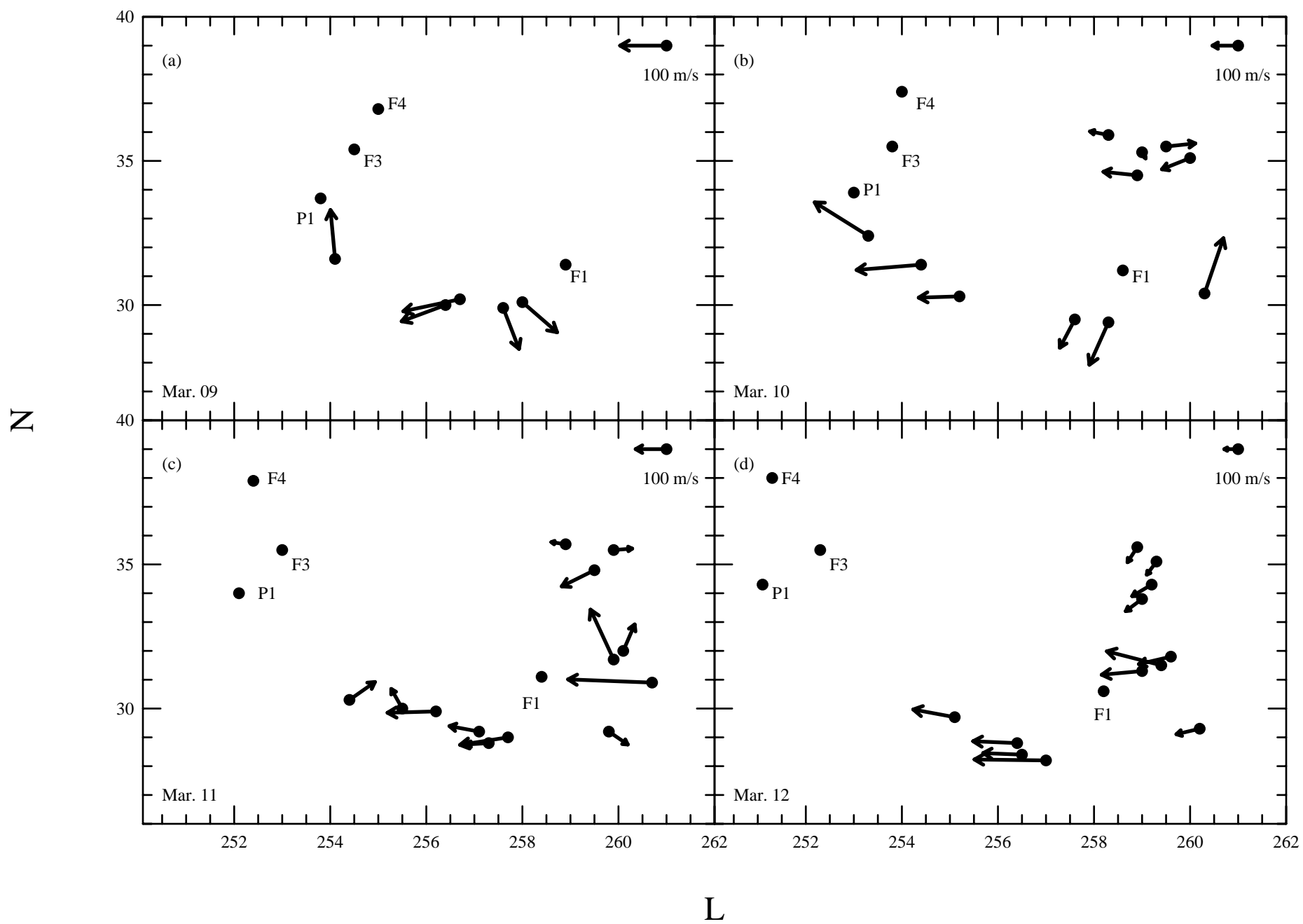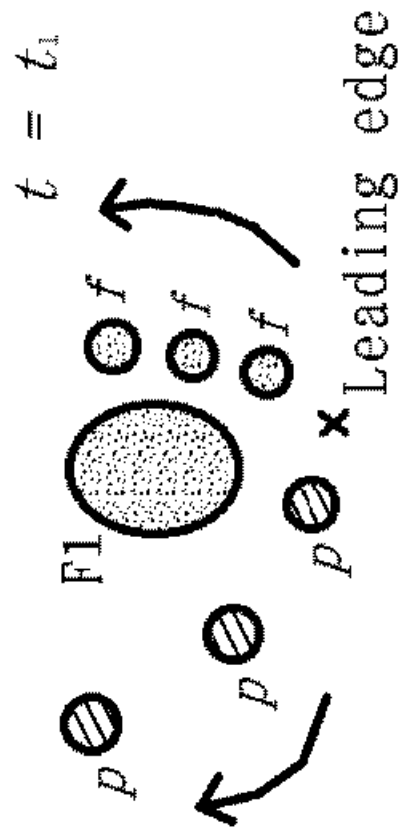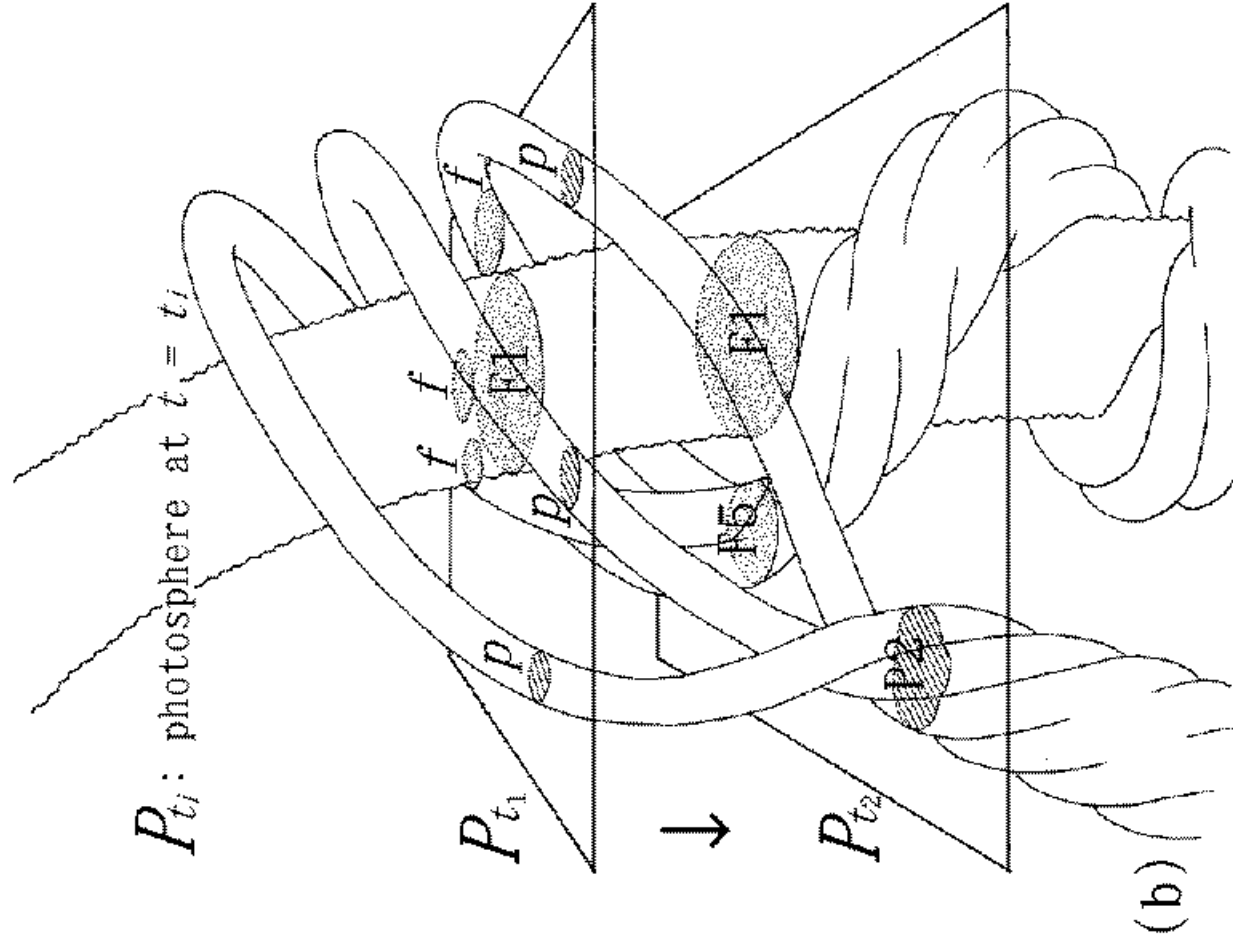
(b)

This figure "fig5.gif" is available in "gif" format from:

http://arXiv.org/ps/astro-ph/9708208v2
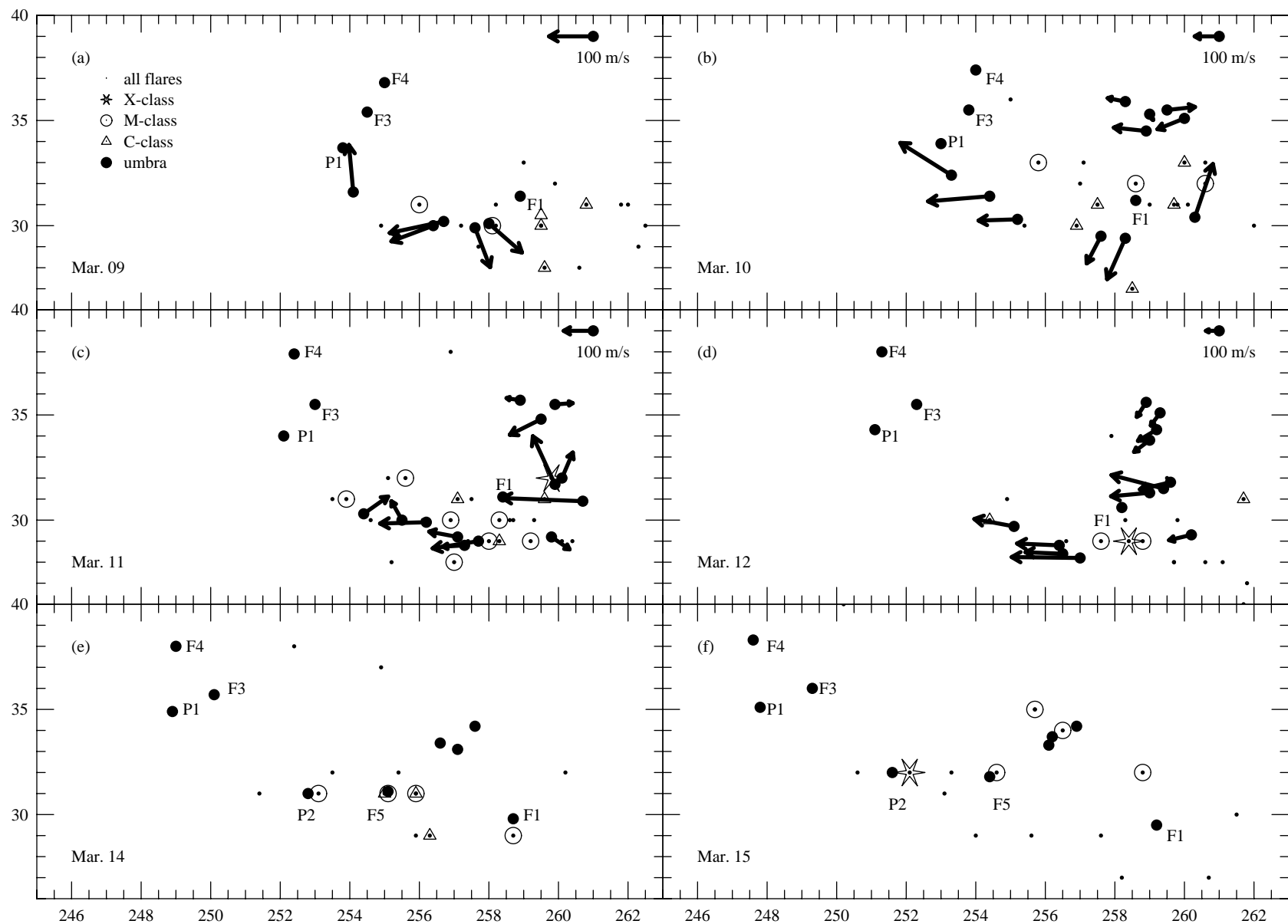
This figure "fig7.gif" is available in "gif" format from:

http://arXiv.org/ps/astro-ph/9708208v2